nature geoscience

ARTICLES

https://doi.org/10.1038/s41561-021-00745-w

Check for updates

Hydrological impact of Middle Miocene Antarctic ice-free areas coupled to deep ocean temperatures

Catherine D. Bradshaw[1,2,3,4] ✉, Petra M. Langebroek[5], Caroline H. Lear[6], Daniel J. Lunt[3], Helen K. Coxall[4], Sindia M. Sosdian[6] and Agatha M. de Boer[4]

Oxygen isotopes from ocean sediments ($\delta^{18}O$) used to reconstruct past continental ice volumes additionally record deep water temperatures (DWTs). Traditionally, these are assumed to be coupled (ice-volume changes cause DWT changes). However, $\delta^{18}O$ records during peak Middle Miocene warmth (~16–15 million years ago) document large rapid fluctuations (~1–1.5‰) difficult to explain as huge Antarctic ice sheet (AIS) volume changes. Here, using climate modelling and data comparisons, we show DWTs are coupled to AIS spatial extent, not volume, because Antarctic albedo changes modify the hydrological cycle, affecting Antarctic deep water production regions. We suggest the Middle Miocene AIS had retreated substantially from previous Oligocene maxima. The residual ice sheet varied spatially more rapidly on orbital timescales than previously thought, enabling large DWT swings (up to 4 °C). When Middle Miocene warmth terminated (~13 million years ago) and a continent-scale AIS had stabilized, further ice-volume changes were predominantly in height rather than extent, with little impact on DWT. Our findings imply a shift in ocean sensitivity to ice-sheet changes occurs when AIS retreat exposes previously ice-covered land; associated feedbacks could reduce the Earth system's ability to maintain a large AIS. This demonstrates ice-sheet changes should be characterized not only by ice volume but also by spatial extent.

Knowledge of Earth's glacial history and evolution through past warm periods is crucial for understanding cryosphere dynamics and future ice-sheet stability. However, the magnitude and timing of ice-sheet variations remains uncertain, even for the largest Cenozoic shifts[1]. Glacial history is commonly reconstructed from the oxygen isotope composition of fossil calcareous benthic foraminifera shells ($\delta^{18}O_c$), a proxy for seawater temperature and ice volume[2]. A rapid coeval increase in global $\delta^{18}O_c$ records is indicative of major ice-growth events. Over the past 40 million years, rapid expansion of the Antarctic ice sheet (AIS) during the Middle Miocene climatic transition (MMCT; ~14–13.8 million years ago (Ma))[3] stands out as one of the three periods of major ice growth in the $\delta^{18}O_c$ record[1].

The MMCT is particularly fascinating because of the hypothesized transition from a less-stable small wet-based AIS[4] where meltwater encourages basal sliding and fast-moving ice to a more-stable large dry-based AIS where the base is frozen to the bedrock[5]. The major ice-growth event is well marked in palaeorecords by an ~1‰ increase in $\delta^{18}O_c$ (Fig. 1), and thereafter, $\delta^{18}O_c$ values have remained at, or above, these levels to the present day[1] because a climatic threshold was crossed[6]. From $\delta^{18}O_c$, inferred MMCT ice growth is equivalent to the size of the entire present-day AIS, or larger[7–11], but ice-sheet isotopic composition changes accounts for some of the amplitude[12,13]. Sequence stratigraphic estimates of sea level (independent from $\delta^{18}O_c$) indicate ~20–60 m changes[14–17]. Previous studies concluded this magnitude of ice growth implies the pre-MMCT AIS volumes must have been very small[18,19]. There is little evidence for notable contemporary Northern Hemisphere glaciation[20], and although Antarctic topography has changed with time because of tectonics, isostatic adjustments and glacial erosion, topographic changes probably account for ~8 m sea-level equivalent (SLE) greater magnitude of ice growth for the same forcing[13], leaving an additional 12–52 m necessary to explain observations.

In stark contrast to the MMCT glaciation, the preceding Miocene Climatic Optimum (MCO; ~16.8–14.8 Ma) contains the lowest $\delta^{18}O_c$ values of the past 25 million years and fossil evidence for notable tundra and woody Antarctic vegetation[21,22] and thereby the globally warmest period/least amount of continental ice. Evidence points to a much reduced size of the dynamic wet-based AIS in the MCO compared with its early Oligocene counterpart[14–17], and large-amplitude $\delta^{18}O_c$ fluctuations combined with sea-level estimates imply a highly dynamic cryosphere (Fig. 1 and Extended Data Fig. 1).

Differing ice growth–DWT relationships

Some key observations from the Middle Miocene Antarctic cryosphere still require explanation. There is a long-held assumption that continental ice volume is inherently coupled to deep water temperatures (DWTs) because expanding ice sheets are assumed to cool high-latitude regions of deep convection[1,3,23]. We would therefore expect both the MCO and MMCT to be associated with DWT changes, yet the $\delta^{18}O_c$ record, combined with independent temperature reconstructions (Fig. 1), reveals some challenging observations. During the MCO, both $\delta^{18}O_c$ and DWT were highly variable (70% of $\delta^{18}O_c$ variability is attributed to changes in DWT[24]). During the MMCT, $\delta^{18}O_c$ was highly variable but DWT variations reduced in amplitude. During the MMCT glaciation, $\delta^{18}O_c$ was highly variable but DWT variations were small (70% of the $\delta^{18}O_c$ variability is attributed to changes in ice volume[24,25]). After the MMCT, $\delta^{18}O_c$ and DWT were variable but less variable than during the MCO.

[1]Met Office Hadley Centre, Fitzroy Road, Exeter, UK. [2]The Global Systems Institute, University of Exeter, Exeter, UK. [3]BRIDGE, School of Geographical Sciences, University of Bristol, Bristol, UK. [4]Department of Geological Sciences, Stockholm University, Stockholm, Sweden. [5]NORCE Norwegian Research Centre, Bjerknes Centre for Climate Research, Bergen, Norway. [6]School of Earth and Environmental Sciences, Cardiff University, Cardiff, UK.
✉e-mail: catherine.bradshaw@metoffice.gov.uk

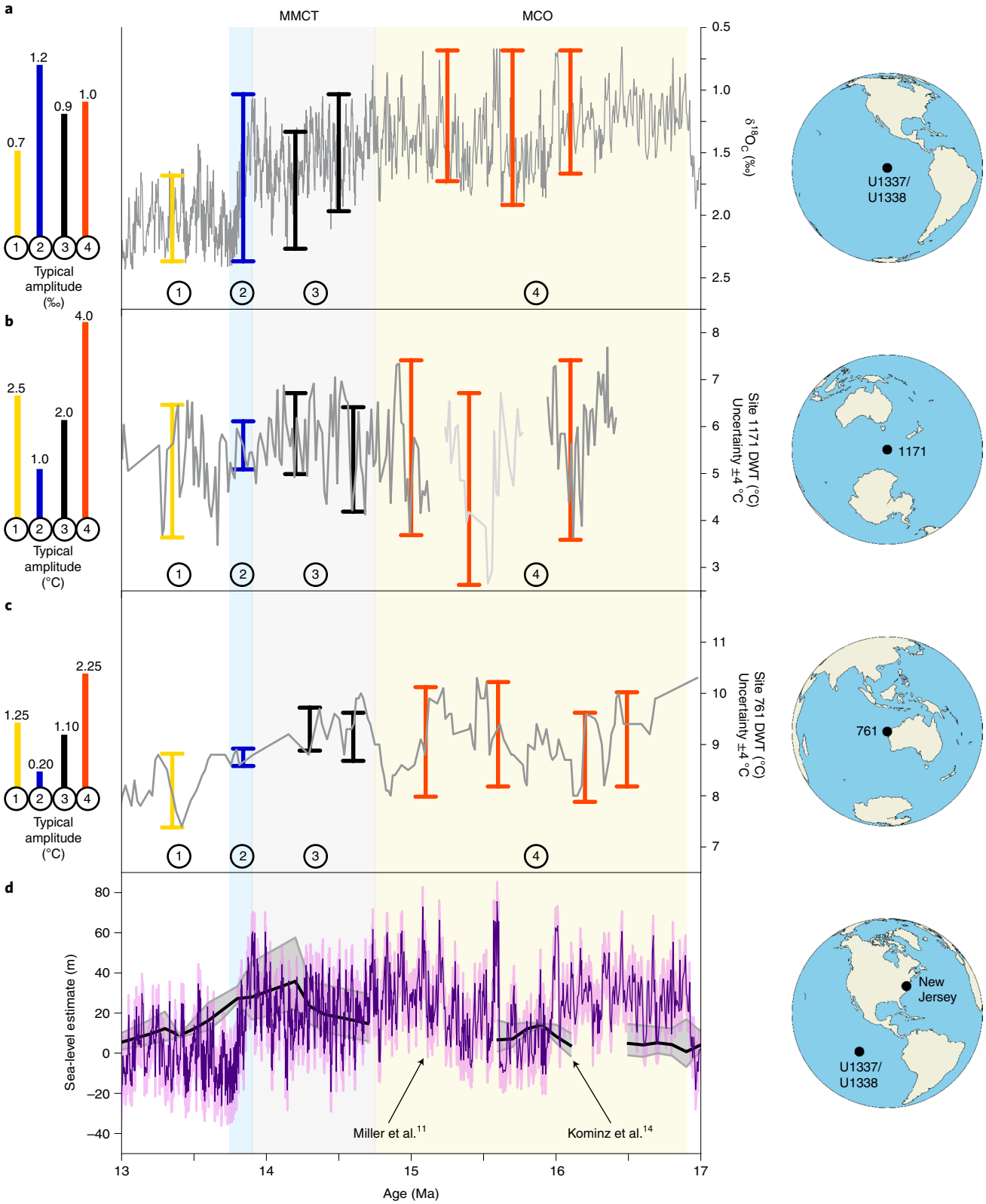

Fig. 1 | Middle Miocene benthic (*Cibicidoides* spp.) oxygen isotope, DWT and sea-level changes. a, $\delta^{18}O_c$ splice[48]. **b**, Site 1171 DWT[25], Southern Ocean (Antarctica-proximal). **c**, Site 761 DWT[8], Indian Ocean (Antarctica-distal but in AABW path). Data locations shown on right of panels. DWTs are Mg/Ca reconstructions (uncertainty ±4 °C; relative values are considered more robust than absolutes). Other available DWT records are too low resolution/short. Data are plotted on their respective age models (full details in Supplementary Table 11). **d**, Sea level[11,14] (eustatic estimates[14] ×1.48 cf. ref. [49]). Shading: MCO, yellow; MMCT, blue and grey; major ice-growth event (MMCT, blue). Vertical lines are indicative of the typical maximum $\delta^{18}O_c$/DWT amplitudes during the MCO (4), MMCT before the major ice-growth event (3), MMCT major ice-growth event (2) and post-MMCT (1). Since the data cover different times and resolutions, these lines are not coincident in time for panels **a**–**c**.

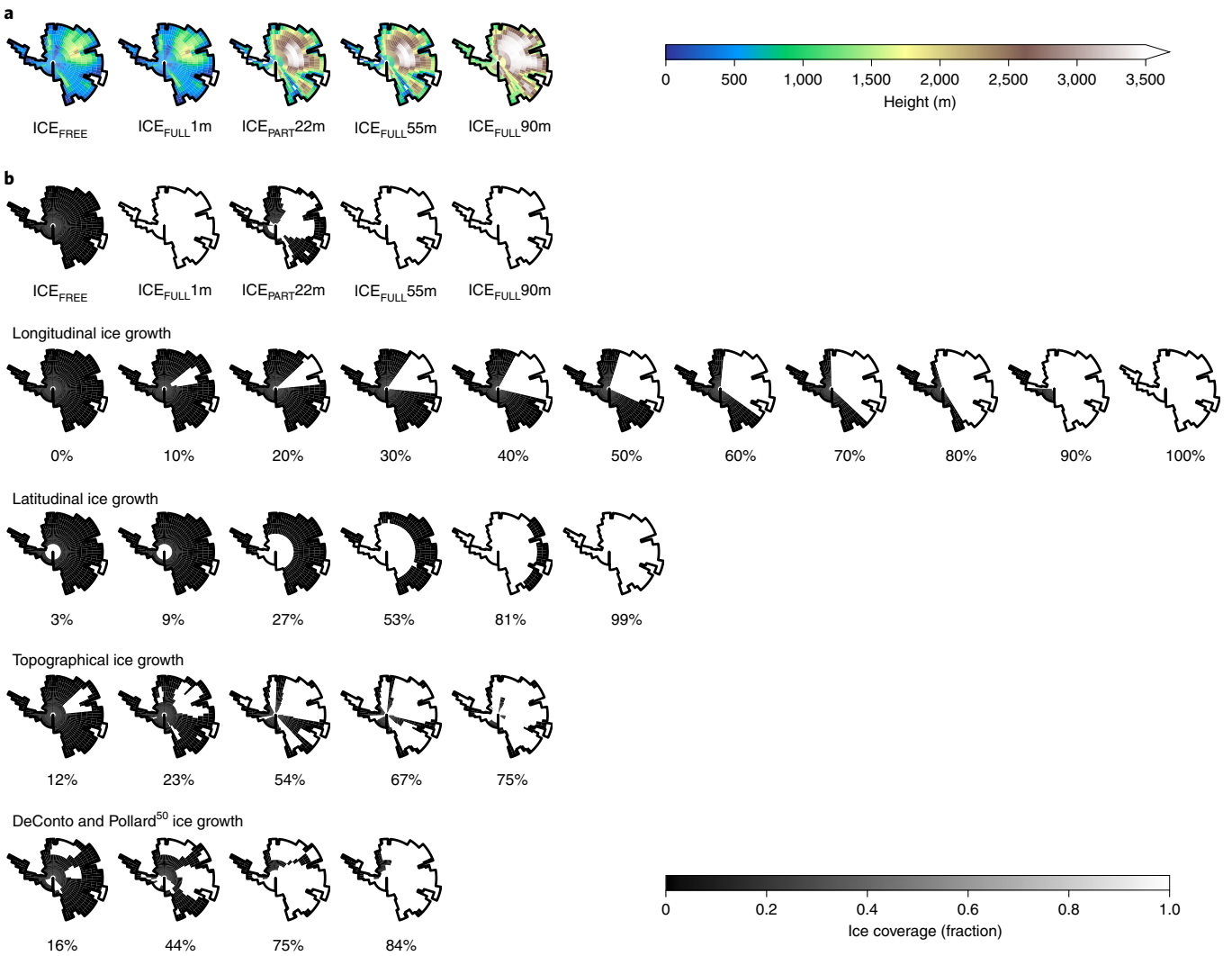

Fig. 2 | Orography and ice-sheet configurations. a, Orography for the different ice-volume scenarios simulated (SLE). **b**, Ice-cover fraction for the different scenarios simulated. The longitudinal, latitudinal, topographical, and DeConto and Pollard[50] ice-sheet extents all use the 1 m SLE orography from **a**. The percentage of ice cover is shown under each thumbnail. Refer also to Methods for more information.

Interpreting $\delta^{18}O_c$ is complicated because both temperature and the ambient seawater isotopic composition ($\delta^{18}O_{sw}$) are recorded. $\delta^{18}O_{sw}$ itself depends on global continental ice volume, the isotopic composition of this ice and localized salinity effects[26]. Paired independent reconstructions can isolate the temperature signal, and analysis of spatially distributed $\delta^{18}O_c$ records can reduce the salinity component. However, for the MMCT glaciation there remains the observation of a large ice increase but little DWT cooling, raising the question of why, if there is a strong coupling between ice volume and DWT as assumed[1,3,23], did DWT vary so much less during the MMCT when ice-sheet growth was most rapid? Here we present new climate model results assessing the impact of ice-sheet size on DWT across the MCO and MMCT. Our results confirm the findings of a previous modelling study that DWT is insensitive to ice-sheet growth at the MMCT[27]. While the previous study explains the MMCT ice volume–DWT decoupling in terms of strong feedbacks in the coupled atmosphere–ocean–sea ice system[27], our study provides further mechanistic understanding of the differing degrees of Middle Miocene ice volume–DWT coupling by proposing a key role for the hydrological cycle. We here advance our understanding of the paradigm by highlighting the important role not only of ice-sheet volume but also of spatial ice-sheet coverage in determining the DWT response to glaciation during the MMCT and the MCO.

We use a fully coupled atmosphere–ocean–vegetation general circulation model, HadCM3LB-M2.1aE[28], configured with Middle Miocene palaeogeography (see Methods and Fig. 2). For our initial assessment using preindustrial CO_2 concentrations, we find that AIS expansion from ice-free (ICE_{FREE}) to the 22 m SLE regional-scale ice-sheet configuration (ICE_{PART}22m) and from ICE_{PART}22m to the 55 m SLE continental ice-sheet configuration (ICE_{FULL}55m) reduces DWT by ~0.5 °C for each step; thus, here, ice growth and DWT are coupled (Fig. 3a). However, AIS expansion from ICE_{FULL}55m to the 90 m SLE continental-scale ice-sheet configuration (ICE_{FULL}90m) does not cause further deep ocean cooling (by contrast, a slight temperature increase is seen); thus, here, ice growth and DWT are decoupled (ice-volume changes do not affect DWT).

We propose that coupling between ice-sheet volume and DWT occurs only until the ice sheet reaches the coast because the ice–albedo feedback mechanism and vegetation–climate interactions invoke additional feedback processes identified here. To demonstrate it is ice-sheet spatial extent (rather than height/volume) that is

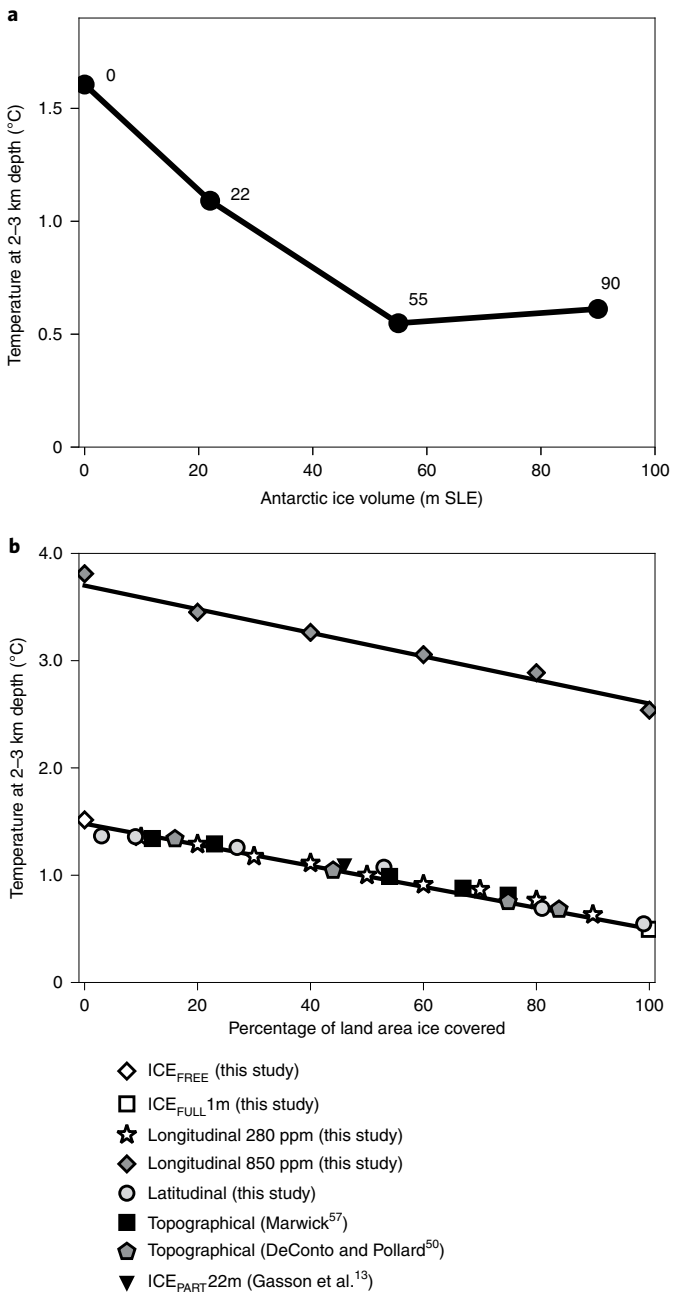

Fig. 3 | Annual mean Southern Hemisphere DWT estimates averaged between 2 and 3 km, simulated with different-sized Antarctic ice sheets. a, Changing ice-sheet volume: ICE_{FREE}, $ICE_{PART}22m$, $ICE_{FULL}55m$ and $ICE_{FULL}90m$. **b**, Changing ice-sheet extent: different scenarios between 0% and 100% ice covered (refer to Fig. 2 for details). CO_2 is 280 ppm in all cases unless specified and a modern orbit assumed; refer to Methods for more information.

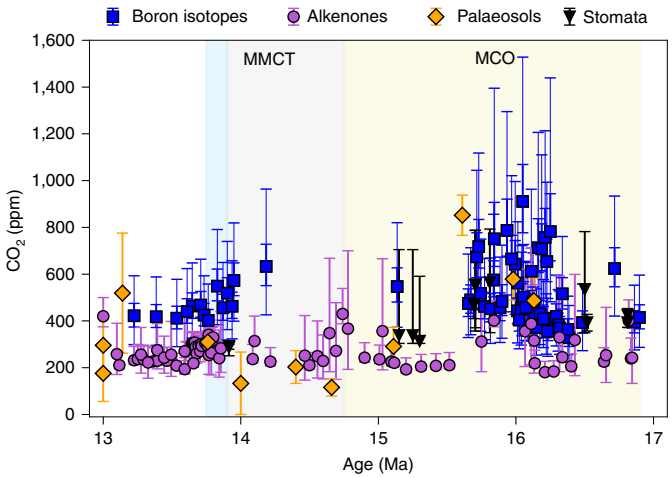

Fig. 4 | Middle Miocene atmospheric CO_2 reconstructions. Data provided in Supplementary Table 5 plotted on respective age models. Shading: MCO, yellow; MMCT, blue and grey; major ice-growth event (MMCT), blue. Note: the plotted Boron isotope-based CO_2 reconstructions from Sosdian et al.[32] are from the L02 scenario and show two error ranges: the 66% (thicker blue lines) and 95% (thinner blue lines) confidence intervals. This dataset supercedes the data from some other publications as documented in Supplementary Table 5 (the reconstructions from the original publications are not plotted).

coupled to DWT, we carry out a non-realistic sensitivity study imposing AIS configurations spanning extreme endmembers from ice-free to ice covered but keep ice volume constant. We assume the ice sheet is of 'skin thickness' (no effective change in elevation as compared with the ice-free state, nominally 1 m SLE when fully ice covered; '$ICE_{FULL}1m$') and vary the ice extent longitudinally, latitudinally and topographically. We use preindustrial CO_2 concentrations throughout and conduct an additional high-CO_2 sensitivity test (~850 ppm; Fig. 4). Combining our results, we find a strong relationship between ice-free extent and DWT, with no evidence of nonlinearity (Fig. 3b).

The mechanism linking ice cover to DWTs

Our modelling results suggest summer 'ice-free' Antarctica (ICE_{FREE}, Fig. 3, column 1) would be warm and wet because the land–sea thermal contrast drives monsoon winds, which transport moisture into the Antarctic continental interior from the Southern Ocean (Fig. 5a–c). This moisture falls over the relatively warm continent as rain, not snow, during the summer months (Fig. 5b) and over much of the continent during the winter months for the two highest CO_2 scenarios. Summer Antarctic temperatures and precipitation are similar to proxy reconstructions for a vegetated Antarctica[4,21,22,29–31]. A comprehensive model–data comparison (Supplementary Note) indicates peak CO_2 would need to be >850 ppm for a complete overlap with proxy reconstructions, in agreement with recent MCO reconstructions[32]. ICE_{FREE} also results in the warmest, freshest deep ocean of all the simulations (Fig. 5d–e). Surface runoff from the active hydrologic cycle, being less saline and thus less dense than the seawater it drains into, forms a polar halocline at the surface. This halocline reduces ventilation of the deep ocean (Fig. 5d), weakening overturning. In our simulations, deep water is in all cases produced primarily in the Southern Ocean; thus, DWTs are determined by southern sinking regions. Antarctic Bottom Water (AABW) production never ceases completely in the model for any scenario (Supplementary Discussion B).

In $ICE_{FULL}1m$, $ICE_{FULL}55m$ and $ICE_{FULL}90m$ (Fig. 5, columns 3–5), cold surface temperatures near the ice sheet and the large increase in albedo cause localized radiative cooling of the air column and a reduction in vapour holding capacity. The land–sea thermal contrast reduces (Fig. 5a), and the summer monsoon system ceases to operate. Katabatic winds form as the cold dense air flows away from the elevated areas towards the coast (Fig. 5c). The interaction between the winds and sea ice is complex and depends on background CO_2 (Fig. 5b and Supplementary Discussion A). Reduced precipitation (Fig. 5b) and subsequent runoff reduce

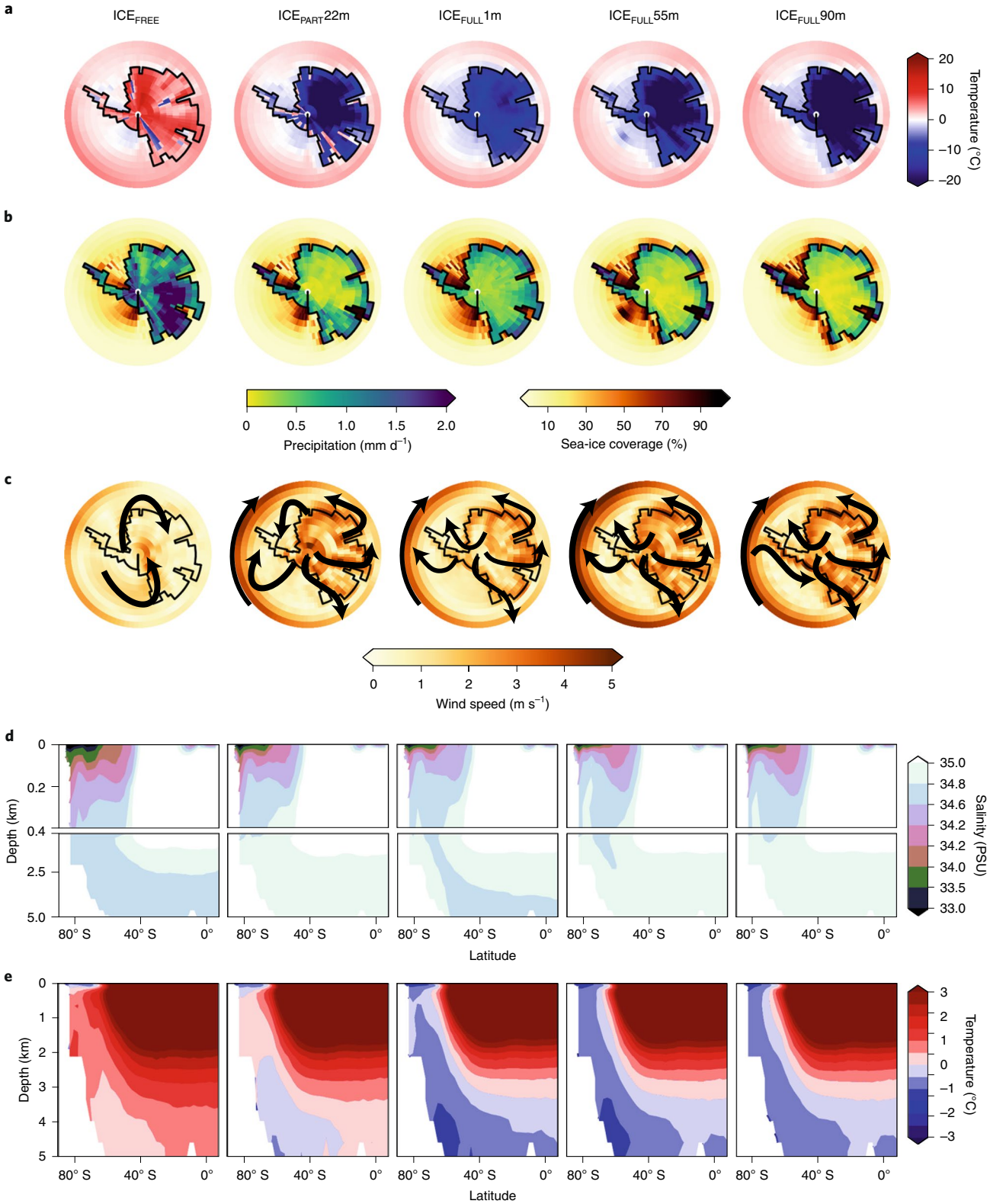

Fig. 5 | Simulated atmospheric and oceanographic conditions with different-sized Antarctic ice sheets. a, Summer (December–January–February) air temperature. **b**, Summer precipitation (land only shown) and sea-ice fraction. **c**, Summer wind speed and prevailing directions. **d**, Annual mean Southern Hemisphere meridional mean ocean salinity. **e**, Annual mean Southern Hemisphere meridional mean ocean temperature. Refer to Methods and Fig. 2 for more details of the boundary conditions used. CO_2 is 280 ppm in all cases.

ocean stratification (Fig. 5d), permitting the cold surface waters to sink more freely from the continental shelf into the abyss (Fig. 5e). Increased AABW production invigorates ocean ventilation.

Empirical studies show a clear relationship between ice-sheet volume and spatial extent[33], implying ice-sheet thickness is limited by spatial extent. Therefore, to grow vertically, an ice sheet must also

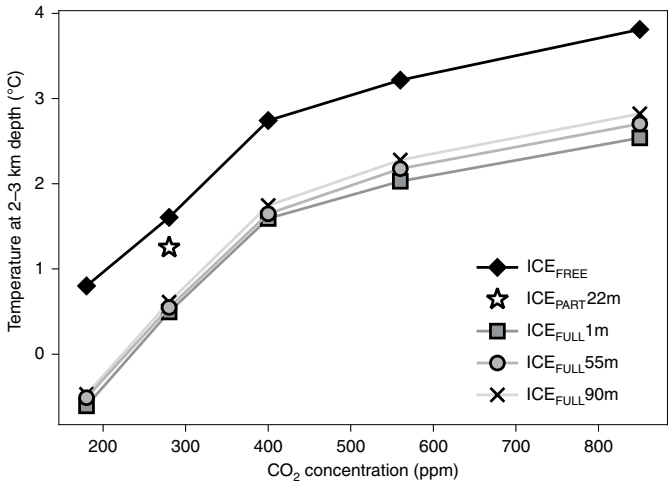

Fig. 6 | Annual mean Southern Hemisphere DWT estimates averaged between 2 and 3 km, simulated with different-sized Antarctic ice sheets and CO_2 concentration. DWTs are averaged between 2 and 3 km water depth. Ice-sheet configurations as in Fig. 5. Refer to Methods and Fig. 2 for more details of the boundary conditions used.

grow spatially (Supplementary Discussion C). After the ice sheet reaches the ocean, additional growth is necessarily predominantly vertical. Although a thickening ice sheet is accompanied by further cooling and drying of the air, this does not markedly affect runoff because precipitation has already been reduced to a low level and is falling as snow, not rain. Consequently, the surface ocean salinity does not change much, and hence, neither does deep water production, ocean ventilation or, crucially, DWT. This explains the ice volume–DWT decoupling among ICE_{FULL}1m, ICE_{FULL}55m and ICE_{FULL}90m. The global mean DWTs begin to rise slowly as ice volume (height) increases (in the absence of CO_2 changes) because the higher topography reduces the amount of summer low clouds around the Antarctic coastline by 10–15% (not shown), allowing more solar radiation to reach the surface and reducing sea ice, which locally causes greater absorption of solar radiation into the ocean.

Our model has a fairly linear response to both a gradually increasing and a decreasing ice-sheet extent. However, we note in a dynamic ice-sheet model, ice melt in the decreasing ice-sheet scenario would result in additional surface runoff that would probably impact AABW production, at least temporarily, as demonstrated in studies of the modern AIS[34].

Sensitivity to atmospheric CO_2 and orbit

Our model does not have an interactive AIS, so the response of the ice sheet to CO_2 forcing is not included, and our study is limited to a single model with mid-range CO_2 sensitivity[35]. However, our results show that atmospheric CO_2 has a much smaller impact on the hydrological regime than ice-sheet configuration (Supplementary Discussion A). CO_2 impacts sea-ice extent and sea surface temperatures, which in turn affect the deeper layers via vertical mixing, in a process that is complex and nonlinear (Supplementary Discussion A).

For the MCO, the most-recent CO_2 record suggests an average range of concentrations between 630 and 470 ppm[32]. Using the relationship between CO_2 and DWT calculated from our simulations, we infer a consequent ~0.8 °C mean temperature change in the 2- to 3-km-deep layer in the Southern Hemisphere (Fig. 6), which is about 80% of the ~1.0 °C impact from increasing ice extent (Fig. 3, ICE_{FULL}1m–ICE_{FREE}) in the same layer. This provides a picture of the average DWT changes. The site-specific temperature changes (of 2–4 °C, Fig. 1), will depend also on local dynamics. At Site 761, our simulations estimate a contribution of 0.5 °C from CO_2 variations compared with a 0.9–1.9 °C contribution from ice-extent changes, and at Site 1171, the contribution from CO_2 is between 0.5 and 0.6 °C compared with 1.0–1.5 °C from ice extent (Supplementary Discussion D,E). Our results show that CO_2 changes alone cannot explain the observed DWT range at the MCO, and moreover, for both the mean layer and the specific sites, our model suggests that ice extent had a larger impact on DWT than did CO_2. For the MMCT glaciation, the most-recent CO_2 reconstructions show at most a 170 ppm reduction from ~570 to 400 ppm[32], for which we infer from our ice-covered model simulations a temperature drop of 0.5–0.8 °C at the two sites (Supplementary Discussion E). This is consistent with the reconstructions (Fig. 1) if we assume Antarctica was ice covered before the MMCT glaciation (that is, little DWT change occurred as a result of increasing ice-sheet extent). In the absence of ice-sheet changes, we find a minimal effect of orbital configuration on DWT (Supplementary Discussion F).

From thin and vulnerable to thick and established

We introduce the hydrological cycle as a crucial mechanism mediating the link between the DWT and the ice spatial extent (rather than absolute volume), thus explaining the different degrees of coupling between ice-sheet changes and DWT during the MMCT and MCO.

Our new results lead us to propose that DWT varied by up to 4 °C during the MCO because the spatial extent of ice and vegetation rapidly altered. Taken together with existing $\delta^{18}O_c$, temperature, vegetation and CO_2 reconstructions, this implies the AIS had retreated substantially during the MCO, when average CO_2 concentrations were probably 470–630 ppm, reaching 780–1,100 ppm at times[32]. Previous work clearly demonstrates the dynamic behaviour of a small AIS when driven by CO_2 changes combined with orbital forcing[7]. How far exactly the ice sheet retreated during these warmest intervals, however, is unknown. Ice-sheet modelling suggests a retreat exposing 60–70% of the Antarctic land surface is consistent with the palaeorecord[13]. Other work concludes a retreat even greater than this[36,37], perhaps even ice-free[11]. The evidence for vegetation, including trees, growing on the continent throughout the MCO[22,29] implies both warm and wet conditions, and it is suggested the moisture supply derived from the Southern Ocean[29]. To achieve this, our results indicate a greater reduction of ice is needed than the ICE_{PART}22m scenario ice-sheet extent because the Wilkes Land winds are directed landward in ICE_{FREE} but seaward for ICE_{PART}22m (Fig. 3c). We suggest these monsoon moisture-carrying winds induced by spatial ice retreat could provide an explanation for major ice advance onto the continental shelf in the Ross Sea[38,39] during the MCO occurring at the same time as open water and woody vegetation in the Wilkes Land[22] (Supplementary Discussion G).

We further infer DWT varied so much less during the MMCT when the AIS volume was growing rapidly because it had already extended to cover most of the continent before the major ice-growth event, in agreement with previous findings[27]. Thus, the ice sheet subsequently increased mainly in thickness, not area, and so DWTs were largely unaffected because, without the additional ice–albedo feedback, changes to the hydrological cycle were much smaller. Post-MMCT (label 1 in Fig. 1), both $\delta^{18}O_c$ and DWT are variable, but less so than during the MCO. The exact degree of coupling, and its mechanism, needs to be explored in a model set-up that includes marine-based ice sheets and ice shelves, not included in this study. However, the physical limits on seawater temperatures (−1.8 °C) will set the lower boundary on possible temperature changes as climate cools.

Interpretation of our results leads us to support a highly dynamic MCO AIS, and state, alongside CO_2, it was changes in ice-sheet area and proximity to the coast, not volume, that were of key importance for global DWTs. This fundamentally changes the way we should characterize ice-sheet changes and how we must view the long-term $\delta^{18}O_c$ records spanning greenhouse–icehouse transitions.

In the absence of independent temperature proxies, it must not be assumed that DWTs scale with ice-volume changes.

While we do not propose the MCO Antarctica was ever completely ice-free, our results demonstrate any spatial retreat of the AIS can increase precipitation, causing associated warming of the deep ocean—changes perhaps having the ability both to accelerate ice melt of ice shelves and glaciers through hydrofracturing from increased precipitation falling into crevasses[40,41] and to accelerate ice melt of marine-based subglacial basins[34,41]. Although the temperature changes resulting from changing ice-sheet extent are similar to those resulting from CO_2 changes, our study does not include feedbacks to the carbon cycle or to the ice sheet itself, and therefore the significance of our results could be greater than indicated here. Our non-realistic sensitivity studies using only a skin thickness of ice demonstrate the importance of both surface albedo and roughness for a hydrologic control on DWT evolution. It is therefore possible that our mechanism could operate in areas even without complete ice loss if these two factors change markedly, for example, in regions of debris-covered glaciers, rock glaciers, vegetation-covered rock glaciers and 'glacier mice', which all increase in the context of retreating ice glaciers[42–45], in regions of accumulating dark particles (dust and soot)[46] and in regions of glacier algae, which bloom in supraglacial meltwater[47].

Online content

Any methods, additional references, Nature Research reporting summaries, source data, extended data, supplementary information, acknowledgements, peer review information; details of author contributions and competing interests; and statements of data and code availability are available at https://doi.org/10.1038/s41561-021-00745-w.

Received: 25 October 2019; Accepted: 24 March 2021;
Published online: 13 May 2021

References

1. Zachos, J., Pagani, M., Sloan, L., Thomas, E. & Billups, K. Trends, rhythms, and aberrations in global climate 65 Ma to present. *Science* **292**, 686–693 (2001).
2. Chappell, J. & Shackleton, N. Oxygen isotopes and sea level. *Nature* **324**, 137–140 (1986).
3. Shackleton, N. J. & Kennett, J. P. in *Initial Reports of Deep Sea Drilling Project* Vol. 29, Report 17 (US Government Printing Office, 1975); https://doi.org/10.2973/dsdp.proc.29.117.1975
4. Lewis, A. R. et al. Mid-Miocene cooling and the extinction of tundra in continental Antarctica. *Proc. Natl Acad. Sci. USA* **105**, 10676–10680 (2008).
5. Kleman, J. & Glasser, N. F. The subglacial thermal organisation (STO) of ice sheets. *Quat. Sci. Rev.* **26**, 585–597 (2007).
6. Levy, R. H. et al. Antarctic ice-sheet sensitivity to obliquity forcing enhanced through ocean connections. *Nat. Geosci.* **12**, 132–137 (2019).
7. Langebroek, P. M., Paul, A. & Schulz, M. Antarctic ice-sheet response to atmospheric CO_2 and insolation in the Middle Miocene. *Clim. Past* **5**, 633–646 (2009).
8. Lear, C. H., Mawbey, E. M. & Rosenthal, Y. Cenozoic benthic foraminiferal Mg/Ca and Li/Ca records: toward unlocking temperatures and saturation states. *Paleoceanography* **25**, PA4215 (2010).
9. Lear, C. H. et al. Neogene ice volume and ocean temperatures: insights from infaunal foraminiferal Mg/Ca paleothermometry. *Paleoceanography* **30**, 1437–1454 (2015).
10. de Boer, B., van de Wal, R. S. W., Lourens, L. J. & Bintanja, R. Transient nature of the Earth's climate and the implications for the interpretation of benthic $\delta^{18}O$ records. *Palaeogeogr. Palaeoclimatol. Palaeoecol.* **335**, 4–11 (2012).
11. Miller, K. G. et al. Cenozoic sea-level and cryospheric evolution from deep-sea geochemical and continental margin records. *Sci. Adv.* **6**, eaaz1346 (2020).
12. Langebroek, P. M., Paul, A. & Schulz, M. Simulating the sea level imprint on marine oxygen isotope records during the Middle Miocene using an ice sheet–climate model. *Paleoceanography* **25**, PA4203 (2010).
13. Gasson, E., DeConto, R. M., Pollard, D. & Levy, R. H. Dynamic Antarctic ice sheet during the Early to Mid-Miocene. *Proc. Natl Acad. Sci. USA* **113**, 3459–3464 (2016).
14. Kominz, M. A. et al. Late Cretaceous to Miocene sea-level estimates from the New Jersey and Delaware coastal plain coreholes: an error analysis. *Basin Res.* **20**, 211–226 (2008).
15. Miller, K. G. et al. The Phanerozoic record of global sea-level change. *Science* **310**, 1293–1298 (2005).
16. Kominz, M. A., Miller, K. G., Browning, J. V., Katz, M. E. & Mountain, G. S. Miocene relative sea level on the New Jersey shallow continental shelf and coastal plain derived from one-dimensional backstripping: a case for both eustasy and epeirogeny. *Geosphere* **12**, 1437–1456 (2016).
17. John, C. M. et al. Timing and magnitude of Miocene eustasy derived from the mixed siliciclastic–carbonate stratigraphic record of the northeastern Australian margin. *Earth Planet. Sci. Lett.* **304**, 455–467 (2011).
18. Pekar, S. F. & DeConto, R. M. High-resolution ice-volume estimates for the Early Miocene: evidence for a dynamic ice sheet in Antarctica. *Palaeogeogr. Palaeoclimatol. Palaeoecol.* **231**, 101–109 (2006).
19. Lear, C. H., Elderfield, H. & Wilson, P. A. Cenozoic deep-sea temperatures and global ice volumes from Mg/Ca in benthic foraminiferal calcite. *Science* **287**, 269–272 (2000).
20. Bierman, P. R., Shakun, J. D., Corbett, L. B., Zimmerman, S. R. & Rood, D. H. A persistent and dynamic East Greenland ice sheet over the past 7.5 million years. *Nature* **540**, 256–260 (2016).
21. Warny, S. et al. Palynomorphs from a sediment core reveal a sudden remarkably warm Antarctica during the Middle Miocene. *Geology* **37**, 955–958 (2009).
22. Sangiorgi, F. et al. Southern Ocean warming and Wilkes Land ice sheet retreat during the Mid-Miocene. *Nat. Commun.* **9**, 317 (2018).
23. De Boer, B., de Wal, R. S. W., Bintanja, R., Lourens, L. J. & Tuenter, E. Cenozoic global ice-volume and temperature simulations with 1-D ice-sheet models forced by benthic $\delta^{18}O$ records. *Ann. Glaciol.* **51**, 23–33 (2010).
24. Kochhann, K. G. D., Holbourn, A., Kuhnt, W. & Xu, J. Eastern equatorial Pacific benthic foraminiferal distribution and deep water temperature changes during the Early to Middle Miocene. *Mar. Micropaleontol.* **133**, 28–39 (2017).
25. Shevenell, A. E., Kennett, J. P. & Lea, D. W. Middle Miocene ice sheet dynamics, deep-sea temperatures, and carbon cycling: a Southern Ocean perspective. *Geochem. Geophys. Geosyst.* **9**, Q02006 (2008).
26. Waelbroeck, C. et al. Sea-level and deep water temperature changes derived from benthic foraminifera isotopic records. *Quat. Sci. Rev.* **21**, 295–305 (2002).
27. Knorr, G. & Lohmann, G. Climate warming during Antarctic ice sheet expansion at the Middle Miocene transition. *Nat. Geosci.* **7**, 376–381 (2014).
28. Valdes, P. J. et al. The BRIDGE HadCM3 family of climate models: HadCM3@ Bristol v1.0. *Geosci. Model Dev.* **10**, 3715–3743 (2017).
29. Feakins, S. J., Warny, S. & Lee, J.-E. Hydrologic cycling over Antarctica during the Middle Miocene warming. *Nat. Geosci.* **5**, 557–560 (2012).
30. Rees-Owen, R. L. et al. The last forests on Antarctica: reconstructing flora and temperature from the Neogene Sirius Group, Transantarctic Mountains. *Org. Geochem.* **118**, 4–14 (2018).
31. Passchier, S. et al. Early Eocene to Middle Miocene cooling and aridification of East Antarctica. *Geochem. Geophys. Geosyst.* **14**, 1399–1410 (2013).
32. Sosdian, S. M. et al. Constraining the evolution of Neogene ocean carbonate chemistry using the boron isotope pH proxy. *Earth Planet. Sci. Lett.* **498**, 362–376 (2018).
33. Paterson, W. S. B. *The Physics of Glaciers* (Elsevier, 2016).
34. Phipps, S. J., Fogwill, C. J. & Turney, C. S. M. Impacts of marine instability across the East Antarctic ice sheet on Southern Ocean dynamics. *Cryosphere* **10**, 2317–2328 (2016).
35. Rugenstein, M. et al. Equilibrium climate sensitivity estimated by equilibrating climate models. *Geophys. Res. Lett.* **47**, e2019GL083898 (2020).
36. Frigola, A., Prange, M. & Schulz, M. Boundary conditions for the Middle Miocene climate transition (MMCT v1.0). *Geosci. Model Dev.* **11**, 1607–1626 (2018).
37. Hamon, N. et al. Growth of subtropical forests in Miocene Europe: the roles of carbon dioxide and Antarctic ice volume. *Geology* **40**, 567–570 (2012).
38. Levy, R. et al. Antarctic ice sheet sensitivity to atmospheric CO_2 variations in the Early to Mid-Miocene. *Proc. Natl Acad. Sci. USA* **113**, 3453–3458 (2016).
39. Colleoni, F. et al. Spatio-temporal variability of processes across Antarctic ice-bed–ocean interfaces. *Nat. Commun.* **9**, 2289 (2018).
40. Van der Veen, C. J. Fracture mechanics approach to penetration of surface crevasses on glaciers. *Cold Reg. Sci. Technol.* **27**, 31–47 (1998).
41. DeConto, R. M. & Pollard, D. Contribution of Antarctica to past and future sea-level rise. *Nature* **531**, 591 (2016).
42. Deline, P. Change in surface debris cover on Mont Blanc massif glaciers after the 'Little Ice Age' termination. *Holocene* **15**, 302–309 (2005).
43. Fickert, T., Friend, D., Grüninger, F., Molnia, B. & Richter, M. Did debris-covered glaciers serve as Pleistocene refugia for plants? A new hypothesis derived from observations of recent plant growth on glacier surfaces. *Arct. Antarct. Alp. Res* **39**, 245–257 (2007).
44. Zale, R. et al. Growth of plants on the late Weichselian ice-sheet during Greenland interstadial-1? *Quat. Sci. Rev.* **185**, 222–229 (2018).

45. Dickson, J. H. & Johnson, R. E. Mosses and the beginning of plant succession on the Walker Glacier, southeastern Alaska. *Lindbergia* **37**, 60–65 (2014).
46. Gölles, T., Bøggild, C. E. & Greve, R. Ice sheet mass loss caused by dust and black carbon accumulation. *Cryosphere* **9**, 1845–1856 (2015).
47. Williamson, C. J. et al. Algal photophysiology drives darkening and melt of the Greenland ice sheet. *Proc. Natl Acad. Sci. USA* **117**, 5694–5705 (2020).
48. De Vleeschouwer, D., Vahlenkamp, M., Crucifix, M. & Pälike, H. Alternating Southern and Northern Hemisphere climate response to astronomical forcing during the past 35 m.y. *Geology* **45**, 375–378 (2017).
49. Pekar, S. F., Christie-Blick, N., Kominz, M. A. & Miller, K. G. Calibration between eustatic estimates from backstripping and oxygen isotopic records for the Oligocene. *Geology* **30**, 903–906 (2002).
50. DeConto, R. M. & Pollard, D. Rapid Cenozoic glaciation of Antarctica induced by declining atmospheric CO_2. *Nature* **421**, 245–249 (2003).

Methods

The model used in these experiments is the fully coupled atmosphere–ocean GCM HadCM3LB-M2.1aE[28] with the interactive vegetation model TRIFFID[51]. This is the low-resolution ocean version of HadCM3[52], and both the atmosphere and the ocean components have a resolution of 2.5° latitude by 3.75° longitude. The model is run without the need for flux adjustments in the modern configuration by the now-standard practice of removing Iceland from the land–sea mask[53]. Eddies in the model are parameterized using a spatially constant coefficient of 1,000 $m^2 s^{-1}$ according to the Gent–Williams scheme[54]. Vertical diffusion is parameterized using the Richardson number-dependent formulation and a background diffusivity of 1×10^{-5} $m^2 s^{-1}$ at the surface, which increases linearly at a rate of 2.8×10^{-8} $m^2 s^{-1} m^{-1}$ with depth[55]. A linear mixing profile with depth has been shown to be able to capture that vertical mixing is strongest over topography[56]. Of all the Paleoclimate Modelling Intercomparison Project (PMIP) 1.5 and PMIP2 models, only the HadCM3-based models, which had such a linear scheme, managed to correctly simulate the Last Glacial Maximum inverse relationship between the volume and production rate of AABW[56]. As such, we have confidence key processes determining the transfer of surface climate signals to depth are represented well in the ocean component of our model.

The background palaeogeography[57] is representative of Middle Miocene conditions. Notable features as compared with modern are that the Panama Gateway and the Indonesian Seaway are open, Australia is located 4° farther south, and the Barents Sea and the Bering Strait are closed. Note that in all experiments, the Eastern Tethys Seaway is also closed. Land topography also differs from modern in that the Tibetan Plateau and the Andes are more than 2,000 m lower than at present, and the Rocky Mountains are about 1,000 m higher. Greenland is also more than 2,000 m lower than modern, and is ice-free.

To investigate Middle Miocene climate, we used a suite of CO_2 and Antarctic ice-cover sensitivity studies. Four Antarctic ice-cover configurations were each simulated at five CO_2 concentrations: 180, 280, 400, 560 and ~850 ppm (in accordance with the uncertainty and temporal variability in CO_2 reconstructions for the Middle Miocene; Fig. 4), giving a total of 20 simulations. The four ice-sheet configurations are defined as follows. First, an ice-free Antarctica using an Antarctic bedrock configuration appropriate for the late Oligocene[57] is referred to as 'ICE_{FREE}.' Ice-free Antarctica is initialized in the Top-down Representation of Interactive Foliage and Flora Including Dynamics (TRIFFID) model as covered in the plant functional type 'shrubs'. Although unrealistic for the Middle Miocene, as the extreme endmember scenario, this scenario helps to place our findings into context. Second, a skin-thickness ice-covered Antarctica (<1 m SLE), where the topography is kept the same as in the ice-free case in 1, is referred to as 'ICE_{FULL}1m'. Third, a modern-like ice-covered Antarctica (~55 m SLE), using the palaeogeographic configuration for the Middle Miocene[57], is referred to as 'ICE_{FULL}55m'. Fourth, a larger-than-modern ice-covered Antarctica (~90 m SLE) is referred to as 'ICE_{FULL}90m'.

The second to fourth configurations have the same areal extent and differ in ice-sheet height only. In accordance with the proposed 90 m drop in sea level over the MMCT[9], boundary conditions for an ice sheet of this proportion were developed by assuming one-third of the ice is associated with isostatic depression and then applying a uniform increase in elevation across the continent to obtain a 90 m SLE. Additionally simulated at 280 ppm (using the topography of the ICE_{FULL}55m scenario) is the spatial extent of the regional-scale ice sheet simulated by a model that includes ice-shelf hydrofracture and ice-cliff collapse of 22 m SLE[13], referred to as 'ICE_{PART}22m'. See Fig. 2 for more details of the Antarctic boundary conditions. Outside of Antarctica, the palaeogeography remains constant at the Middle Miocene reconstruction. Apart from the prescribed CO_2 changes, all other greenhouse gases and solar and orbital parameters remain at modern settings.

To investigate the sensitivity of the hydrological cycle to the extent of Antarctic ice-free area, an additional series of simulations were carried out with a gradually increasing Antarctic ice-sheet area, from no ice to the maximum ice-sheet extent for the second scenario in the preceding. These intermediate-area ice sheets expand latitudinally, longitudinally or topographically as demonstrated in Fig. 2. No change was made to the elevation from the ice-free condition, and therefore all of these simulations represent a skin thickness of ice cover. Two sets of scenarios were run for each of the longitudinal ice-growth boundary conditions. First, beginning from an ice-free initial condition (as described in the preceding) and second, beginning from a 100% ice-covered initial condition and decreasing towards zero. The rest of the scenarios were initiated from the 100% ice-covered state and therefore lose ice only. The longitudinal ice-growth scenario also included four configurations simulated at ~850 ppm CO_2 (20%, 40%, 60% and 80% ice covered; refer to Fig. 2).

All simulations assume a modern orbit except for four sensitivity test cases. A cold orbital configuration favourable for Antarctic glaciation (low obliquity (22.1°), high eccentricity (0.054), perihelion during boreal summer, 374 W m^{-2} summer insolation at 70° S) and a warm orbital configuration favourable for Antarctic deglaciation (high obliquity (24.5°), high eccentricity (0.054), perihelion during austral summer, 483 W m^{-2} summer insolation at 70° S) were identified. Cold and warm orbit sensitivity tests were carried out for the ICE_{FREE} and the ICE_{FULL}55m configurations.

All of the Middle Miocene simulations continue from a 2,100-year integration under late Miocene boundary conditions[58] and have been run for a further 2,000 years. Supplementary Figs. 65–68 show the evolution of DWTs throughout the simulations and give us confidence that they have stabilized sufficiently for us to draw conclusions.

Data availability

The climate model output data are available for analysis and download at https://www.paleo.bristol.ac.uk/ummodel/scripts/papers/Bradshaw_et_al_2021.html. It is possible to reproduce the information in Figs. 2, 3, 5 and 6 via this interface as well as download the data itself and the ancillary information (palaeogeography and ice-sheet configuration).

Code availability

The UK Met Office made available the source code of HadCM3 via the Ported Unified Model release (https://www.metoffice.gov.uk/research/approach/collaboration/unified-model/partnership). Enquiries regarding the use of HadCM3 should be directed in the first instance to the UM Partnership team, who can be contacted at um_collaboration@metoffice.gov.uk. The main repository for the Met Office Unified Model (UM) version corresponding to the model presented here can be viewed at http://cms.ncas.ac.uk/code_browsers/UM4.5/UMbrowser/index.html (registration required). The code detailing the changes required to update HadCM3 to HadCM3LB-M2.1 are available as a supplement to Valdes et al.[28].

References

51. Cox, P. M. *Description on the TRIFFID Dynamic Global Vegetation Model* Technical Report 24 (Hadley Centre, Met Office, 2001).
52. Gordon, C. et al. The simulation of SST, sea ice extents and ocean heat transports in a version of the Hadley Centre coupled model without flux adjustments. *Clim. Dyn.* **16**, 147–168 (2000).
53. Jones, C. A fast ocean GCM without flux adjustments. *J. Atmos. Ocean. Technol.* **20**, 1857–1868 (2003).
54. Gent, P. R. & McWilliams, J. C. Isopycnal mixing in ocean circulation models. *J. Phys. Oceanogr.* **20**, 150–155 (1990).
55. Pacanowski, R. & Philander, S. Parameterization of vertical mixing in numerical models of tropical oceans. *J. Phys. Oceanogr.* **11**, 1443–1451 (1981).
56. De Boer, A. M. & Hogg, A. M. Control of the glacial carbon budget by topographically induced mixing. *Geophys. Res. Lett.* **41**, 4277–4284 (2014).
57. Markwick, P. J. in *Deep-Time Perspectives on Climate Change: Marrying the Signal from Computer Models and Biological Proxies* (eds Williams, M. et al.) 251–312 (The Geological Society, 2007).
58. Bradshaw, C. D. et al. The relative roles of CO_2 and palaeogeography in determining Late Miocene climate: results from a terrestrial model–data comparison. *Clim. Past* **8**, 715–786 (2012).

Acknowledgements

C.D.B. and D.J.L. were supported by NERC grant NE I006281/1. C.H.L. and S.M.S. were supported by NERC grant NE/I006427/1. A.M.deB. and C.D.B. gratefully acknowledge support from the Swedish Research Council project [2016-03912]. This work was carried out using the computational facilities of the Advanced Computing Research Centre, University of Bristol: http://www.bristol.ac.uk/acrc/. We thank D. Suri, chief operational meteorologist, Met Office; G. Guentchev, senior scientist, Met Office; S. Feakins; and T. Naish for feedback on earlier drafts of this manuscript. We also thank E. Gasson for providing a plot of his ice-sheet model results[13].

Author contributions

C.D.B., C.H.L. and D.J.L. conceived the project and directed the research with the assistance of A.M.deB.; C.D.B. conducted and interpreted the modelling with the assistance of D.J.L., A.M.deB. and P.M.L.; C.D.B compiled and interpreted the proxy records with the assistance of C.H.L., A.M.deB., H.K.C. and S.M.S.; C.D.B. led the writing of the paper. All authors contributed to writing the manuscript.

Competing interests

The authors declare no competing interests.

Additional information

Extended data is available for this paper at https://doi.org/10.1038/s41561-021-00745-w.

Supplementary information The online version contains supplementary material available at https://doi.org/10.1038/s41561-021-00745-w.

Correspondence and requests for materials should be addressed to C.D.B.

Peer review information *Nature Geoscience* thanks Sarah Feakins, Tim Naish and the other, anonymous, reviewer(s) for their contribution to the peer review of this work. Primary Handling Editor: James Super.

Reprints and permissions information is available at www.nature.com/reprints.

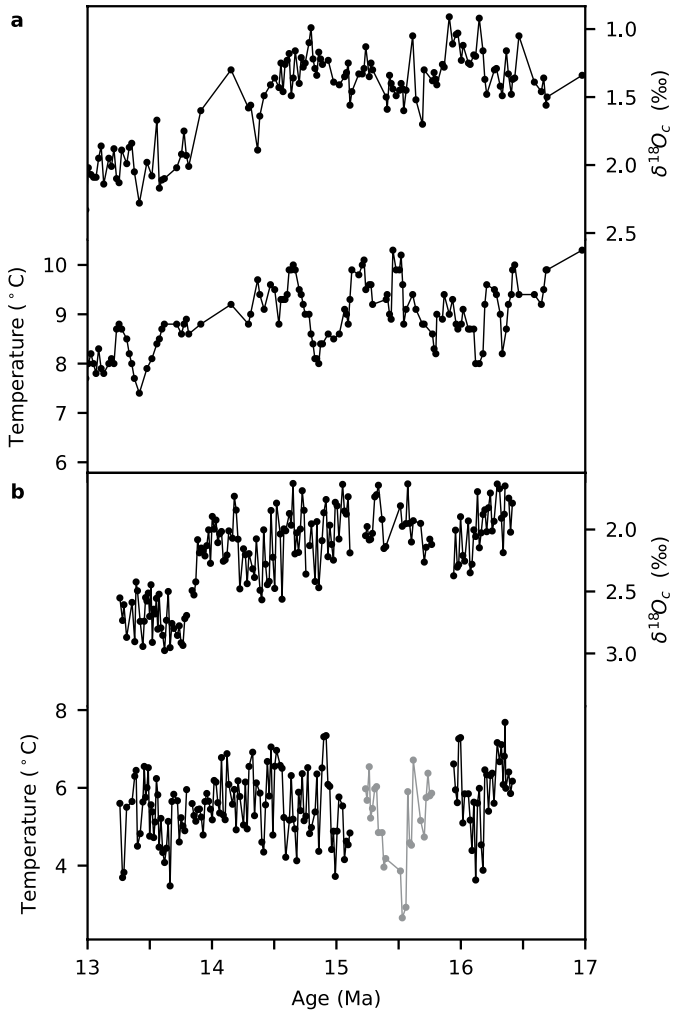

Extended Data Fig. 1 | Benthic (*Cibicidoides spp.*) oxygen isotope $\delta^{18}O_c$ and deep water temperatures (DWT) changes from the Mg/Ca proxy through the Middle Miocene. a Site 761 in the Indian Ocean[8], **b** Site 1171 in the Southern Ocean[25]. Data are plotted on their respective age models. DWT uncertainty is ±4 °C; relative values are considered more robust than absolutes.